Turkish Journal of Electrical Engineering & Computer Sciences

http://journals.tubitak.gov.tr/elektrik/

Research Article

Turk J Elec Eng & Comp Sci
(2018) 26: 347 – 362

doi:10.3906/elk-1703-101

Supercapacitor utilization for power smoothening and stability improvement of a hybrid energy system in a weak grid environment

Rahul SHARMA*, Sathans SUHAG
Department of Electrical Engineering, National Institute of Technology, Kurukshetra, India

Received: 09.03.2017 • **Accepted/Published Online:** 20.06.2017 • **Final Version:** 26.01.2018

Abstract: In this paper, a novel control scheme based on the application of a supercapacitor (SC) is proposed for power smoothening and stability improvement of a hybrid energy system (HES) in weak grid conditions. The basic property of fast charging/discharging of the SC is utilized to design the proposed control. In weak grid conditions, the control structure is proposed for power smoothening and DC link voltage regulation with the help of the SC. Moreover, the stability is increased, ripples in voltage are reduced, there is fast dynamic response, and oscillations are damped out under different conditions. In conventional control, voltage controller stability is the main concern under weak grid conditions. On the other hand, the proposed control scheme has independent voltage controller stability in weak grid conditions. Drawbacks of the conventional scheme due to coupling components and large grid impedance in a weak grid are illustrated mathematically. The design and the steady-state stability analysis of the proposed control scheme are explained and compared with the conventional scheme. The HES is modeled and simulated in MATLAB/Simulink to verify the enhanced performance of the proposed scheme. In comparison with the conventional control strategy, the proposed scheme has an improved DC link voltage profile and smoothened power, resulting in the fast dynamic response of the HES connected to the weak grid.

Key words: Supercapacitor, hybrid energy system, power quality, photovoltaic, weak grid, stability

1. Introduction

In the present scenario, power generation using alternate energy sources is becoming very important because of the sharp rise in consumption, depleting fossil fuels and creating environmental concerns. Under such circumstances, renewable energy sources are the most viable alternatives to meet the future demand globally, but renewable energy sources have their own limitations [1]. Different renewable energy-based configurations such as standalone, grid-connected, and microgrid-based systems have been reported in the literature to ensure continuous, reliable, and quality power supply. The recent literature suggests that a hybrid energy system (HES) connected to a microgrid offers one of the better possible solutions in the present scenario [2]. However, there are many stability and control challenges that need to be addressed [3]. Stability and power quality are the main concerns in a weak grid environment because of the low short-circuit ratio (SCR) and significant grid impedance [4]. Therefore, attention is needed to mitigate the voltage fluctuations and the ripple in power and, at the same time, to improve transients, dynamic response, and stability of the system. The above issues have to be addressed to provide quality power.

In the recent literature, some control strategies are proposed to increase the stability margin and improve

*Correspondence: rahulsharma.knit2006@gmail.com

power quality under weak grid conditions. Control loop modeling is the most common practice applied to the analysis of the stability of a weak grid-connected inverter [5]. Grid-connected and islanding mode control is discussed to suppress the voltage fluctuation under transition periods, but it compromises steady-state response where ripples are present in the power because of the coupling components [6]. Improved control strategy is proposed for weak grid-connected inverters using adaptive control but system stability is affected where local constant and dynamic AC/DC loads are also connected to the point of common coupling (PCC) [7]. Therefore, different current controllers are implemented, such as repetitive and harmonic resonant controllers used to enhance the stability margin of the inverter connected to a weak grid [8]. If the grid impedance is assumed as a part of the LCL filter, proper damping and stability are improved. However, the grid impedance is a variable parameter and cannot be measured. Therefore, the transient and dynamic responses deteriorate and stability may be lost under the grid impedance fluctuations [9]. Similarly, notch filters are used to design the current control loop for active damping, but the coupling terms make distortion in the current waveform and worsen the power quality [10]. Therefore, the feedforward approach with adaptive control of the parameter adjustment has been provided as a better solution to improving the decoupling of the coupling terms and stability within a weak grid [11,12]. The grid impedance is considered in the control loop in the analysis of the stability margin, applying the control loop modeling method. However, the parameter design of the coupling terms is difficult. In consequence, the behavior of the system under sudden changes is adversely affected in terms of transient and dynamic responses [13]. Moreover, a weak grid poses challenges to improve the behavior of the transient and dynamic response as well as stability due to the impact of AC bus voltage control on DC link voltage control [14]. Therefore, a weak grid not only adversely affects the regulation of active power by DC link voltage control but also causes interactions between other control loops that affect system voltage dynamics [15].

This paper proposes a novel control scheme to address the problems of a HES connected to a weak grid in different operating conditions. The HES has to be able to provide power in grid-connected as well as standalone conditions for better utilization. The energy storage devices in the HES are used to maintain the DC link voltage constant under standalone/islanding mode only, whereas, in grid-connected mode, no energy storage device is utilized in the system. Unlike conventional control, in this paper, the SC, as an energy storage device, is used to participate in the inverter control of the system connected to the weak grid also.

The proposed scheme maximizes the utilization of the SC by its participation in grid-connected mode. This paper only utilizes the basic property of the SC to design the proposed control. Therefore, the structure and manufacturing differences of the different types of SCs are not within the scope of the paper and are not discussed [16].

In this paper, the control scheme is proposed, by using a SC in grid-connected mode, to:

1. Increase the stability margin under weak grid conditions.
2. Regulate DC link voltage and achieve better transient and dynamics of the HES.
3. Improve power quality by reducing ripples due to lower order harmonics.

This paper is divided into five sections. Section 2 covers the analysis and design of the conventional and proposed control schemes for a HES in weak grid conditions. Section 3 includes the stability analysis of the conventional and proposed control schemes. Section 4 demonstrates the simulation results of the HES in different conditions and provides a comparison of the results with the conventional scheme. Lastly, Section 5 concludes the findings of this study by highlighting the effectiveness of the proposed control scheme.

2. System description and control scheme

The proposed control scheme, implemented on a HES, consists of a PV panel as a renewable energy source, a SC as an energy storage device, and power electronics converters as power conditioning devices, as shown in Figure 1.

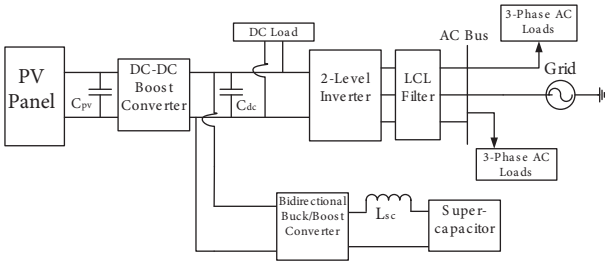

Figure 1. Schematic diagram of hybrid energy system.

Figure 2 shows the configuration of the inverter connected to the grid through an LCL filter with the SC connected to the DC link of the inverter. The Buck-boost DC-DC converter is utilized to control the SC output, which consists of inductance L_{sc} and bidirectional switches SW_3/SW_4, where i_{sc} is SC current, d_{sc} is duty cycle, and v_{sc} is SC voltage. The LCL filter consists of L_1, L_2, and C_f as configured in Figure 2. The detailed design of the LCL filter has been reported in the literature [17].

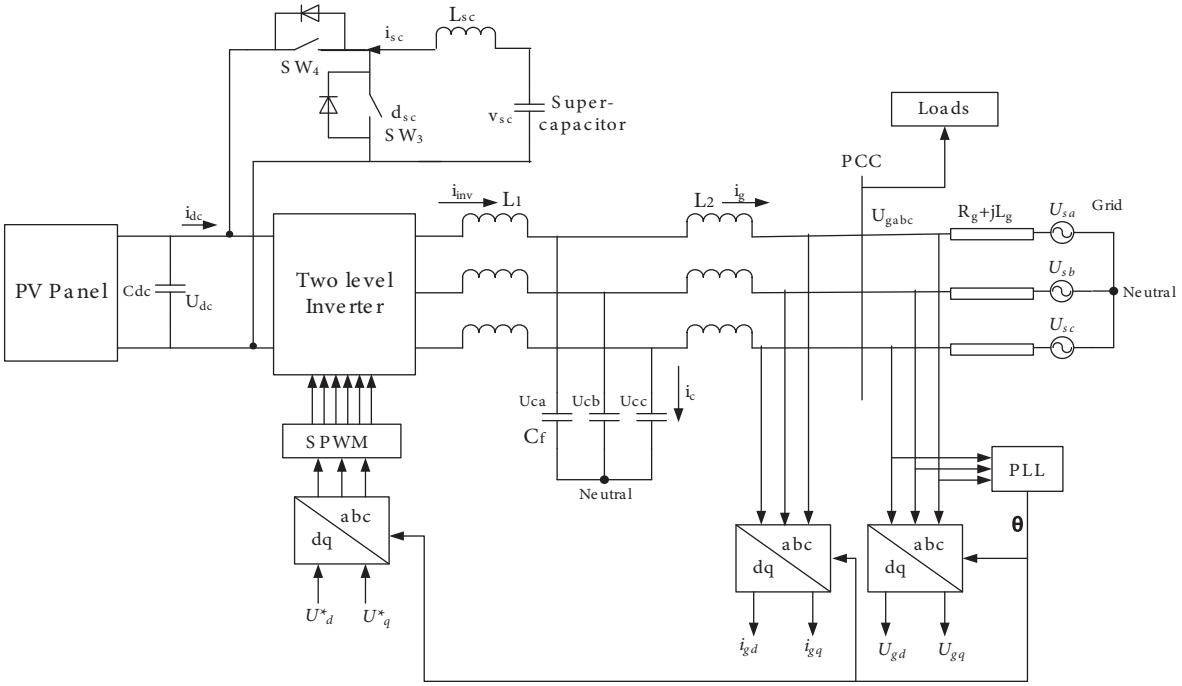

Figure 2. Structure of weak grid-connected inverter with LCL filter and SC.

At the PCC, local loads and the grid are connected, where U_{sabc} is grid Thevenin voltage, R_g is grid resistance, L_g is grid inductance, Z_g is grid impedance, i_g is injected current into the grid, i_c is capacitor current, i_{inv} is inverter side current, i_{dc} is the input current of the inverter, and U_{gabc} is grid voltage at the PCC. Park's transformation is used to transform the stationary reference frame (abc) into the synchronous reference frame ($dq0$). Grid voltage is measured for the feedforward and phase-locked loop (PLL) function.

2.1. Conventional control structure for HES connected to weak grid

Conventional control of the grid-connected LCL inverter [18] is shown in Figure 3 to control DC link voltage U_{dc} across capacitance C_{dc} and reactive power. $U*_{dc}$ is the reference DC link voltage, where reference d-axis grid current $i*_{gd}$ is the output of the DC link voltage controller while $i*_{gq}$ is the reference q-axis grid current chosen as zero to regulate reactive power for unity power factor. $U*_d$ and $U*_q$, which are the outputs of the grid current control loops, are taken as the voltage references. The impacts of the grid resistance and switching losses are negligible (even resistance is improved by the stability of the control very slightly) in the control scheme [19]. Therefore, switching losses and grid resistance are taken as negligible just to design the proposed control and stability analysis of the inverter under weak grid conditions because resistance and switching losses do not affect the stability of the inverter. In the power circuit, impedance has significant inductive and resistive values and switching loss is also considered. In this modeling, grid voltage is assumed to be sinusoidal and balanced. Transformation of the equations from the stationary to synchronous reference frame has been done using the grid voltage angle as a reference. Now the equations of inverter voltages U_d and U_q can be written as:

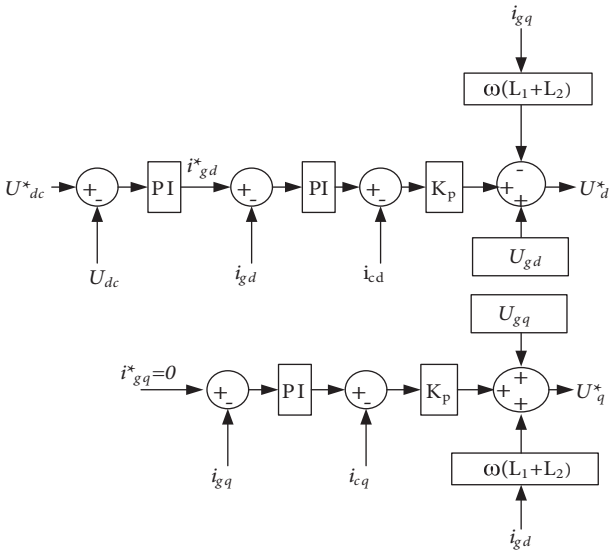

Figure 3. Conventional control scheme for grid-connected inverter.

$$U_d = L\frac{di_{gd}}{dt} + U_{gd} - \omega L i_{gq}, \tag{1}$$

$$U_q = L\frac{di_{gq}}{dt} + U_{gq} + \omega L i_{gd}, \tag{2}$$

where $L = L_1 + L_2$ and ω is the angular frequency. With the help of the feedforward method, the output of the current controller ΔU is added to get reference voltages as:

$$U^*_d = \Delta U_d + U_{gd} - \omega L i_{gq}, \tag{3}$$

$$U^*_q = \Delta U_q + U_{gq} + \omega L i_{gd}. \tag{4}$$

However, in the grid, where the SCR is less than three and grid impedance is significant and has to be taken into account in order to draw a valid conclusion, also known as weak grid conditions, the conventional control

scheme is not appropriate to provide quality power output to be injected into the weak grid due to the reasons analyzed as follows:

1. Under transient response, changes in load/input power would change the grid current to maintain the voltage constant, directly reflected in reference currents as:

$$i_{gd}^{*} = \Delta i_{gd} + i_{gd}, \tag{5}$$

$$i_{gq}^{*} = \Delta i_{gq} + i_{gq}, \tag{6}$$

where Δi_{gd} and Δi_{gq} are the values of current that get added up in the previous grid current values and directly reflected into the reference currents. These changes do not get directly reflected in the feedforward decoupled components $-\omega L i_{gq}$ and $\omega L i_{gd}$; as a result, the dynamic response of the grid current control loop is slow.

2. Voltage controller stability is the main concern in weak grid conditions where the grid impedance is an unknown variable over a wide range and depends on operating conditions. The voltage control loop is the outer loop and the grid current control loop is the inner loop. The bandwidth of the voltage control loop is maintained less than the grid current control loop because the voltage control loop is slower than the current control loop. Therefore, in a weak grid case where the grid impedance is considered, the feedforward decoupled control must compensate for $-\omega L i_{gq} - \omega L_g i_{gq}$ and $\omega L i_{gd} + \omega L_g i_{gd}$. Therefore, Eqs. (3) and (4) can be written as:

$$U_d^{*} = \Delta U_d + U_{gd} - \omega L i_{gq} - \omega L_g i_{gq}, \tag{7}$$

$$U_q^{*} = \Delta U_q + U_{gq} + \omega L i_{gd} + \omega L_g i_{gd}. \tag{8}$$

However, L_g is unknown grid inductance and therefore cannot be compensated using feedforward decoupled control. As a result, coupling components of grid inductance reduce the current control loop stability margin. Therefore, in the conventional approach, under large values of grid inductance L_g, feedforward decoupled control seriously compromises the robustness of the current control loop in weak grid conditions. The stability of the voltage controller is adversely affected due to the dependency of the proportional-integral (PI) controller gain on the inner grid current control loop. Therefore, under large inductance variations, the controller becomes unstable.

3. Steady-state ripples also remain present in the grid current as nonlinear loads inject lower order harmonics at steady state, which the conventional control scheme is not able to suppress. Therefore, grid current at steady state can be written as:

$$i_{gd} = i_{gd}^{*} + \hat{i}_{gd}, \tag{9}$$

$$i_{gq} = i_{gq}^{*} + \hat{i}_{gq}, \tag{10}$$

where $\hat{i_{gd}}$ and $\hat{i}_{gq}$ are the steady-state ripple currents. These steady-state ripples reduce the waveform quality of the grid current. Furthermore, ripple current components affect the coupling terms. Now reference voltages can be written as:

$$U_d^{*} = \Delta U_d + U_{gd} - \omega L i_{gq} - \omega L \hat{i}_{gq}, \tag{11}$$

$$U_q^* = \Delta U_q + U_{gq} - \omega L i_{gd} - \omega L \hat{i}_{gd}. \tag{12}$$

As the reference voltages contain the terms $-\omega L\hat{i}_{gq}$ and $\omega L\hat{i}_{gd}$ as per Eqs. (11) and (12), this will interact and worsen the waveform quality of the current and power further.

2.2. Proposed control structure for HES connected to weak grid

Figure 4 shows the proposed control scheme of the HES for the grid-connected mode. This scheme involves an outer voltage control loop, inner grid current control loop (for d- and q-axis), and inner SC current control loop. The SC has a fast charging/discharging rate; hence, the dynamic response of the SC control loop is faster than the grid current control loop [20]. Therefore, the SC current control loop is utilized to compensate for transients and steady-state ripples in power. To utilize SC fast dynamic characteristics, the SC current control loop is designed and the developed relations between all control loops are determined by mathematical analysis. Now the reference grid current $i*_{gd}$ is generated by the outer voltage control loop. Furthermore, the reference grid current is separated by the low-pass filter (LPF) into two components as average current component (DC value) $i*_{gd\_LF}$ and high frequency current component $i*_{gd\_HF}$. Therefore, reference grid current can be written as:

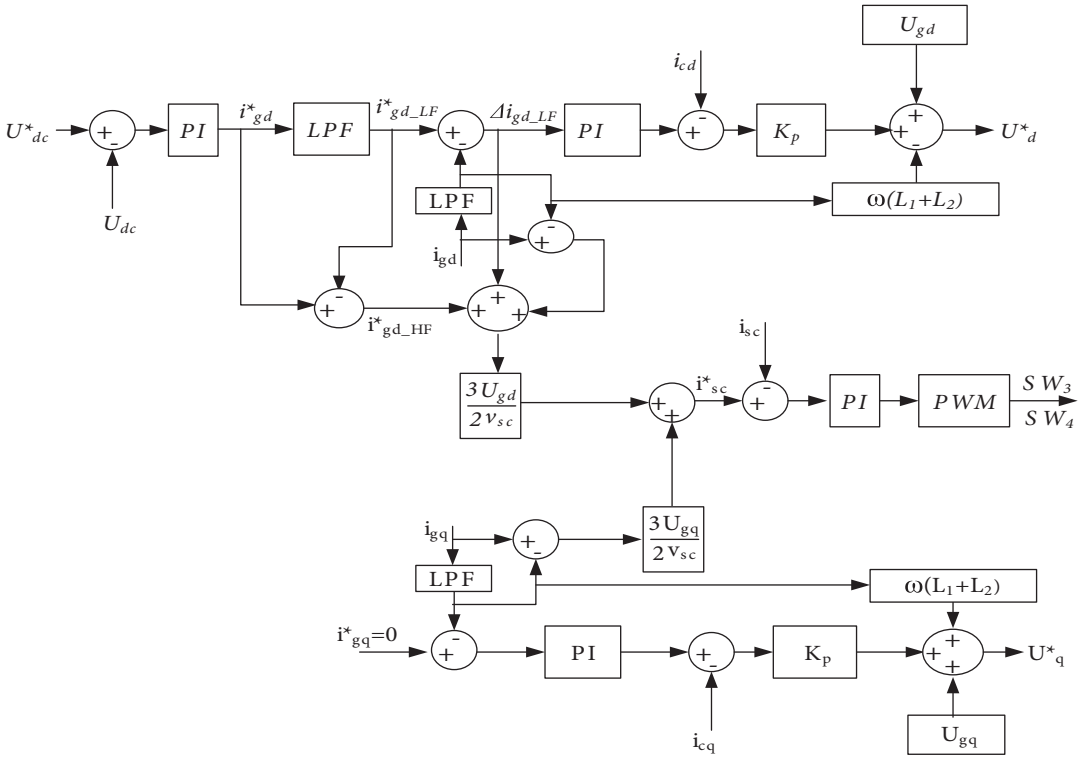

Figure 4. Proposed control scheme of HES for grid-connected mode.

$$i_{gd}^* = i_{gd\_LF}^* + i_{gd\_HF}^*, \tag{13}$$

$$i_{gq}^* = i_{gq\_LF}^* + i_{gq\_HF}^*. \tag{14}$$

Under transient conditions, reference grid current $i*_{gd}$ contains DC value $i*_{gd\_LF}$ and high frequency current component $i*_{gd\_HF}$. Now reference power $p*_g$ is needed to be injected into the grid for power balancing and

DC link voltage regulation, whereas p_g is the actual power being injected into the grid and can be written as:

$$p_g = \frac{3}{2}(U_{gd}i_{gd} + U_{gq}i_{gq}), \tag{15}$$

whereas

$$p_g^* = \frac{3}{2}(U_{gd}i_{gd}^* + U_{gq}i_{gq}^*). \tag{16}$$

However, $i_{gq}^* = 0$; therefore, $p_g^* = \frac{3}{2}U_{gd}i_{gd}^*$ and from Eq. (13) can be written as:

$$p_g^* = \frac{3}{2}(U_{gd}i_{gd\_LF}^* + U_{gd}i_{gd\_HF}^*). \tag{17}$$

Eq. (17) can be rewritten with the help of Eq. (5) as:

$$p_g^* = \frac{3}{2}(U_{gd}i_{gd\_LF} + U_{gd}\Delta i_{gd\_LF} + U_{gd}i_{gd\_HF}^*). \tag{18}$$

Now, as per Eq. (18), the reference power comprises three components to be injected into the grid, which are $\frac{3}{2}U_{gd}i_{gd\_LF}$, the actual power component without steady-state ripples; $\frac{3}{2}U_{gd}\Delta i_{gd\_LF}$, the DC value of change in power; and $\frac{3}{2}U_{gd}i_{gd\_HF}^*$, the high frequency component responsible for ripples under transient conditions, where, i_{gd_LF} is the low frequency d-axis grid current. Besides the actual power component, the additional power required for compensation is:

$$p_{un\_comp} = \frac{3}{2}U_{gd}\Delta i_{gd\_LF} + \frac{3}{2}U_{gd}i_{gd\_HF}^*, \tag{19}$$

where $\frac{3}{2}U_{gd}i_{gd\_HF}^*$ is the high frequency component, which does not exist in a steady-state condition but must be damped out as early as possible to improve transient response. The grid current control loop cannot damp out the high frequency component; however, the SC current control loop is able to compensate for the high frequency component by its inherent characteristics of fast charging/discharging. Therefore, this component is compensated by the SC. Similarly, the $\frac{3}{2}U_{gd}\Delta i_{gd\_LF}$ component is compensated by the grid current control loop, but it takes a long time due to the slow dynamic response of the grid current control loop. Therefore, initially, this component is compensated by the SC current control loop to improve the dynamic response of the voltage control loop.

Under steady-state conditions, ripples are present in the grid current due to lower frequency harmonics. Therefore, the grid current can be written as:

$$i_{gd} = i_{gd\_LF}^* + \hat{i}_{gd}, \tag{20}$$

$$i_{gq} = i_{gq\_LF}^* + \hat{i}_{gq}. \tag{21}$$

Ripple currents can be extracted by the LPF under the steady state. Ripples are high frequency components, whereas steady-state grid currents are DC values. Therefore,

$$p_{ripple} = \frac{3}{2}(U_{gd}\hat{i}_{gd} + U_{gq}\hat{i}_{gq}). \tag{22}$$

Steady-state ripple currents inject ripples in the power, which get reflected in the form of ripples in the DC link voltage. These ripples can be damped out by compensating ripple power p_{ripple} with the help of a SC current control loop.

Now the total compensating power p_{comp} needed to compensate for transients and ripples can be written as:

$$p_{comp} = \frac{3}{2}U_{gd}(\Delta i_{gd\_LF} + i^*_{gd\_HF} + \hat{i}_{gd}) + \frac{3}{2}U_{gq}\hat{i}_{gq}. \tag{23}$$

Therefore, SC reference current i^*_{sc} can be obtained as:

$$i^*_{sc} = \frac{3}{2}\frac{U_{gd}}{v_{sc}}(\Delta i_{gd\_LF} + i^*_{gd\_HF} + \hat{i}_{gd}) + \frac{3}{2}\frac{U_{gq}}{v_{sc}}\hat{i}_{gq}. \tag{24}$$

With the help of Eq. (24), the proposed control scheme is shown in Figure 4 where the output of the SC current control loop generates the switching signal for bidirectional buck-boost converter switches SW_3 and SW_4 while the inner grid current control loops generate the signal to control inverter switches. This proposed control has the risk that if the SC state of charge (SOC) is below the lower cutoff or above the upper cutoff then the proposed control is not able to regulate the DC link voltage properly. Therefore, to avoid such situations, the SOC limits are also used to generate the switching signal of buck-boost converter switches SW_3 and SW_4. If SOC is greater than 0.9 or below 0.2, then both switches SW_3 and SW_4 are turned off and the proposed control behaves as a conventional control scheme to avoid any adverse effect on the system.

3. Design and stability analysis

3.1. Conventional control scheme

The stability of the conventional control scheme is analyzed by considering voltage control loop bandwidth to be less as compared to inner current control loop bandwidth because the voltage PI controller is tuned based on the inner current control loop. Figure 5 shows the mathematical model of inverter current control connected to the weak grid, which consists of the inner loop proportional regulator and the outer loop PI regulator. Switching frequency f_s of the inverter is taken as 10 kHz, where, $G_c(s)$ is the gain of the outer loop PI regulator, K_p is the gain of the proportional regulator, and K_{pwm} is the gain of the inverter.

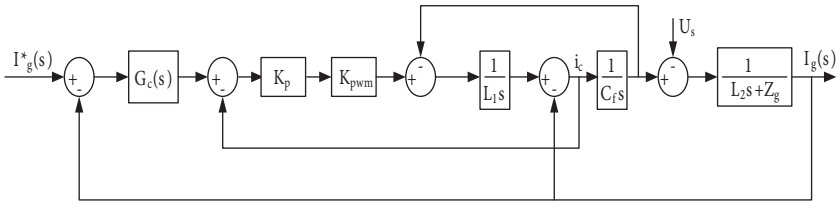

Figure 5. Mathematical model of weak grid-connected inverter current control.

According to Figure 5, the closed loop transfer function is:

$$G_{cl\_i}(s) = \frac{I_g(s)}{I^*_g(s)} = \frac{G_c(s)K_pK_{pwm}}{L_1C_f(L_2+L_g)s^3 + K_1s^2 + K_2s + K_3}, \tag{25}$$

where $K_1 = (L_2 + L_g)C_fK_pK_{pwm}$, $K_2 = L_1 + L_2 + L_g$, and $K_3 = G_c(s)K_pK_{pwm}$.

The open loop transfer function of the voltage control loop can be derived as per Figure 6, where, $G_v(s)$ is the gain of the PI voltage controller and $G_{cl\_i}(s)$ is the grid current closed loop control gain.

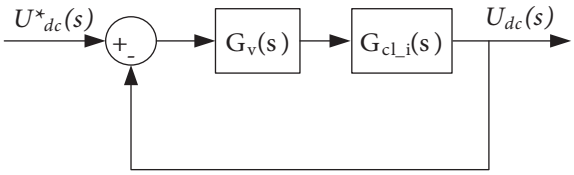

Figure 6. Block diagram of voltage controller with conventional control scheme.

Now the voltage control loop has three controller gains, $G_v(s)$, $G_c(s)$, and K_p, where $G_v(s)$ and $G_c(s)$ can be written as:

$$G_v(s) = K_{p\_v} + \frac{K_{i\_v}}{s}, \tag{26}$$

$$G_c(s) = K_{p\_c} + \frac{K_{i\_c}}{s}. \tag{27}$$

Therefore, the open loop transfer function $G_{ol\_v}(s)$ of the voltage control loop can be written as:

$$G_{ol\_v}(s) = G_v(s)G_{cl\_i}(s). \tag{28}$$

The controllers are designed to achieve high bandwidth and a good stability margin. The parameters of the controller are obtained by diagram-aided method. The diagram-aided method is basically a computer-based single-input, single-output (SISO) tool in MATLAB to obtain the parameters with the help of defining the system transfer function. The SISO tool gives the bode and root locus plot where the poles and zeros can be adjusted to get the desired output and corresponding parameters of the controller [21]. The values of controller gains so obtained are as follows: $K_p = 10.6$, $K_{p\_c} = 7.2$, $K_{i\_c} = 12{,}000$, $K_{p\_v} = 0.221$, $K_{i\_v} = 110.36$, where K_{pwm} is assumed as unity. Now the phase margin (P.M.) and gain margin (G.M.) are 103° and 15 dB, respectively, as obtained in MATLAB from the open loop bode plot of $G_{ol\_v}(s)$ when the value of grid inductance is $L_g = 0$. The open loop bode plots are shown in Figure 7 with different values of grid inductance L_g for voltage control loop.

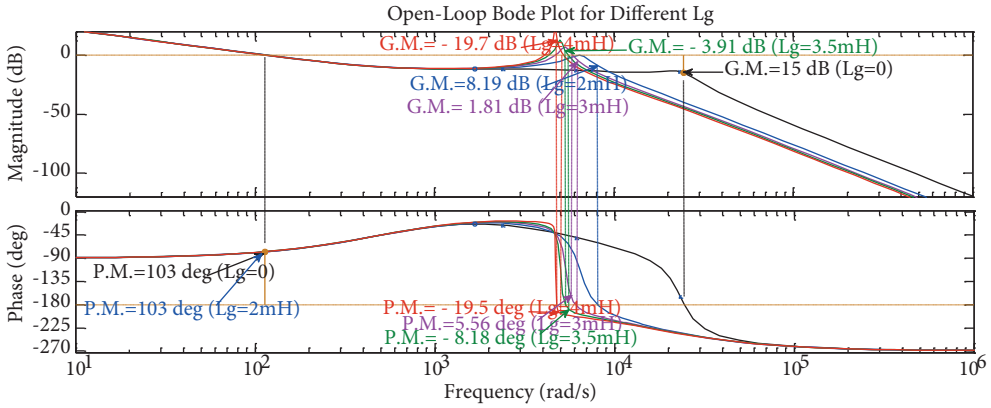

Figure 7. Bode plots of the voltage control loop.

Now the impact of the grid impedance on the stability of the voltage control loop in the conventional scheme is analyzed. The impact of the grid resistance is negligible in the control scheme. Therefore, assuming $r_g = 0$, the effect of L_g is studied. When $L_g = 2$ mH, phase and gain margins are 103° and 8.19 dB, respectively,

which provides reasonably good stability margins, but the margins get reduced as compared to the case when the value of L_g is considered as zero. Similarly, at L_g = 3 mH, the voltage control loop stability margins decrease sharply as P.M. and G.M. are 5.56° and 1.81 dB, respectively. The voltage control loop becomes unstable when L_g = 3.5 mH, 4 mH, or more, where both phase and gain margins are negative. Under weak grid conditions, stability analysis shows that the conventional scheme does not provide good stability margins.

3.2. Proposed control scheme

In the proposed control scheme, voltage and grid current control loops are designed and their stabilities are analyzed separately because both loops are independent of each other. The SC current control loop is faster than the grid current control loop; therefore, the voltage control loop is tuned based on the SC current control loop. Figure 8 shows the SC current control loop, where $G_{pi\_sc}(s)$ is the gain of the PI regulator and $G_{id\_sc}(s)$ is the gain of the bidirectional DC/DC buck-boost converter [22].

Therefore, $G_{pi\_sc}(s)$ and $G_{id\_sc}(s)$ can be written as:

$$G_{pi\_sc}(s) = K_{p\_sc} + \frac{K_{i\_sc}}{s}, \tag{29}$$

$$G_{id\_sc}(s) = \frac{U_{dc}C_{dc}s + 2i_{dc}}{L_{sc}C_{dc}s^2 + (U_{dc}/i_{dc})L_{sc}s + (1-d_{sc})^2}. \tag{30}$$

Now the closed loop transfer function of SC current control $G_{cl\_sc}(s)$ can be written as:

$$G_{cl\_sc}(s) = \frac{G_{pi\_sc}(s)G_{id\_sc}(s)}{1 + G_{pi\_sc}(s)G_{id\_sc}(s)}. \tag{31}$$

Figure 9 shows the voltage control loop, based on the SC current control loop, comprising $G_v(s)$ as PI regulator gain, $G_{cl\_sc}(s)$ as transfer function of closed loop SC control loop, and $G_{v\_dc}(s)$ as the transfer function of SC inductor current to DC link voltage [22].

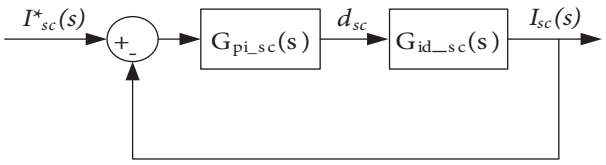

Figure 8. Block diagram of SC current controller.

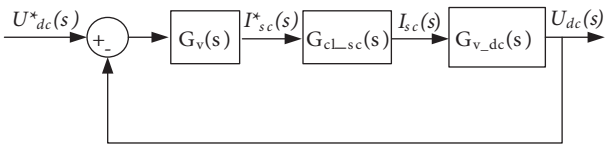

Figure 9. Block diagram of voltage controller with proposed control scheme.

Therefore, $G_v(s)$ and $G_{v\_dc}(s)$ can be written as:

$$G_v(s) = K_{p\_v} + \frac{K_{i\_v}}{s}, \tag{32}$$

$$G_{v\_dc}(s) = \frac{(U_{dc}/i_{dc})(1-d_{sc})(1 - \frac{L_{sc}s}{(U_{dc}/i_{dc})(1-d_{sc})^2})}{2 + (U_{dc}/i_{dc})C_{dc}s}. \tag{33}$$

From Eqs. (31), (32), and (33), the open loop transfer function of the voltage control loop, $G_{ol\_v}(s)$, can be written as:

$$G_{ol\_v}(s) = G_v(s)G_{cl\_sc}(s)G_{v\_dc}(s). \tag{34}$$

Hence, Eq. (34) shows that the transfer function of the voltage control loop is totally independent of L_g. Controllers are designed for high bandwidth and good stability margins by using the diagram-aided method. The details of controller gains obtained are as follows: $K_p = 10.6$, $K_{p\_c} = 4.09$, $K_{i\_c} = 6193$, $K_{p\_sc} = 0.005$, $K_{i\_sc} = 5$, $K_{p\_v} = 0.077$, $K_{i\_v} = 77$, and K_{pwm} is taken as unity. Figure 10 shows the open loop bode plots of the voltage control loop, which has good phase and gain margins, as 76.6° and 10 dB, respectively. Now the phase and gain margins of the voltage control loop are totally independent of grid inductance. Therefore, the proposed voltage control scheme provides absolute stability and robustness even under very large values of grid inductance. Open loop bode plots of the grid current control loop with different values of L_g are shown in Figure 11.

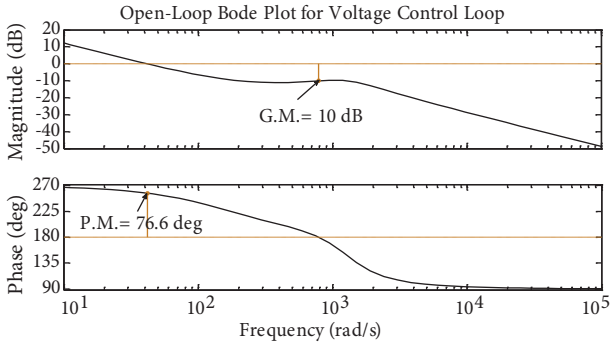

Figure 10. Bode plot of the voltage control loop.

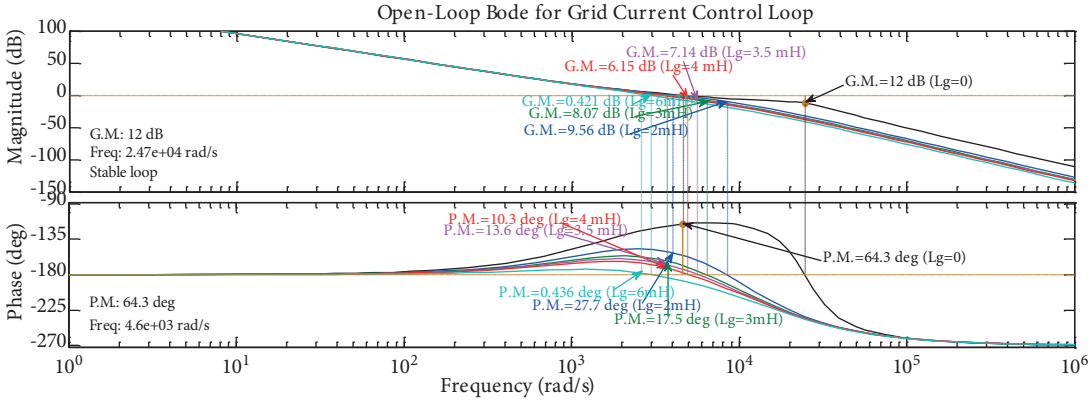

Figure 11. Bode plots of grid current control loop with different L_g.

Large variations in grid inductance are taken from $L_g = 0$ to 6 mH to analyze the stability of the grid current control loop. Unlike the conventional control scheme, the grid current control loop in the proposed scheme provides a much better stability margin even with large values of L_g.

4. Results and discussion

The proposed control scheme has been implemented in a 100 kW hybrid renewable energy system with a PV panel under weak grid conditions. To demonstrate the performance of the proposed scheme, the system is simulated in MATLAB under different operating conditions. The system parameters are given in the Table.

Solar irradiance and load changes are introduced to assess the system performance under different operating conditions. To verify the performance of the proposed scheme, the results under a weak grid are

Table. Storage device parameters and nominal system parameters.

Supercapacitor	58 F, 16 V, 20 no. connected in series	PV system rating	100 kW
Nominal DC link voltage,U_{dc}	450 V	Ac bus voltage rating, v_p	270 V
L_{sc},L_{pv}	5 mH, 5 mH	X_g/R_g	< 3
v_{sc}	320 V	L_1	0.35 mH
C_{pv}	100 μF	L_2,R_g	0.1 mH, 1 Ω
C_{dc}	1000 μF	C_f	120 μF

discussed and compared with that of conventional control. Figure 12 shows the waveform of variations of irradiance as input to the PV panel.

Figure 13 shows the waveforms of DC link voltage with the proposed and conventional control schemes. It is evident that, under transient conditions, the waveform of DC link voltage with the proposed scheme indicates better transient response as DC link voltage regulation is faster and the waveform exhibits relatively smaller oscillations, but in the conventional scheme, the voltage has large oscillations and slow response when being regulated.

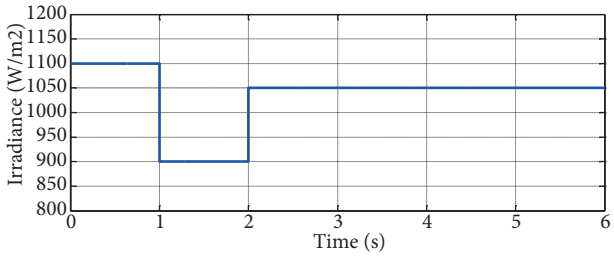

Figure 12. Waveform of variation of solar irradiance.

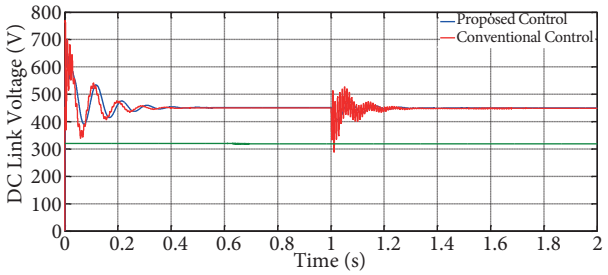

Figure 13. Waveform of DC link voltage and SC voltage.

Figure 14 shows the DC link voltage under different grid inductance values with conventional control. As is clearly visible, the waveform is adversely affected by an increase in grid inductance. On the other hand, the proposed control scheme provides better DC link voltage as shown in Figure 15; the waveform is smooth with improved dynamic response under transient conditions with different values of grid inductance.

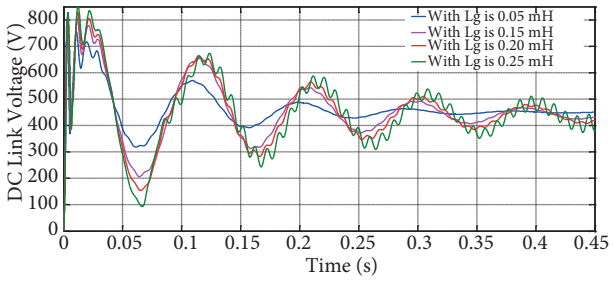

Figure 14. DC link voltage with conventional control scheme.

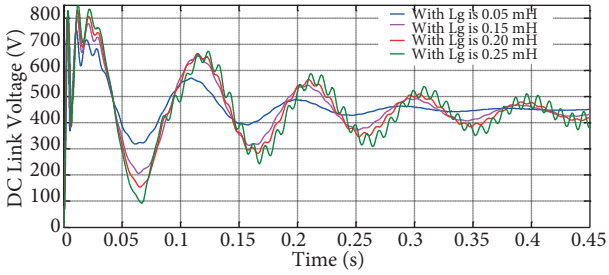

Figure 15. DC link voltage with proposed control scheme.

Figure 16 shows the variations of the d-axis and SC current under transient conditions; initially the SC current regulates the DC link voltage and balances the power, which improves the overall transient and dynamic response of the system.

In Figure 17, three-phase grid voltages are shown with the proposed and conventional control schemes, where, under transient conditions at 1 s, the grid voltage is constant and the disturbance is negligible with the proposed control scheme, whereas with the conventional control scheme grid voltage is distorted significantly and gets reestablished after a long time.

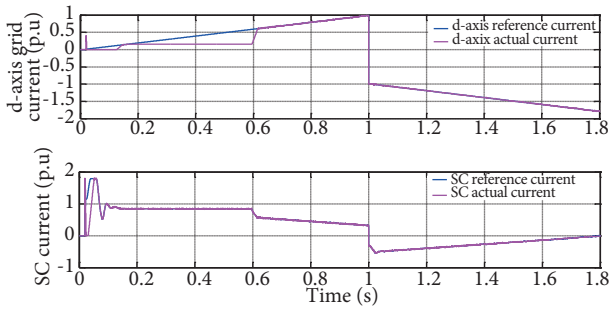

Figure 16. d-axis grid current and SC current.

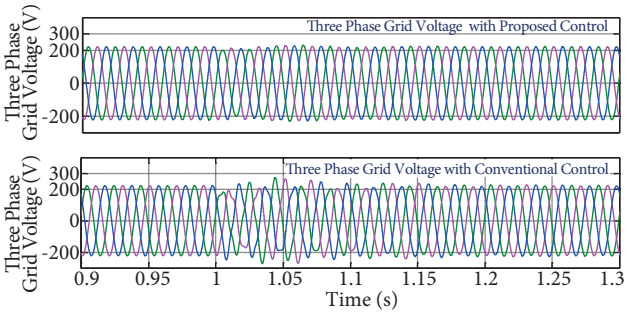

Figure 17. Transient behavior of the three-phase grid voltage waveform.

Similarly, in Figure 18, three-phase grid current waveforms with the proposed and conventional control schemes are shown. The proposed control scheme improves the transient response of grid current and the change in grid current is smooth under a change in operating conditions, but the same is not true with conventional control where the waveform of the grid current is distorted.

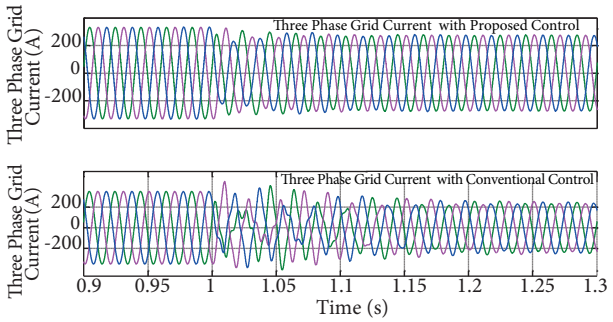

Figure 18. Transient behavior of the three phase grid current waveform.

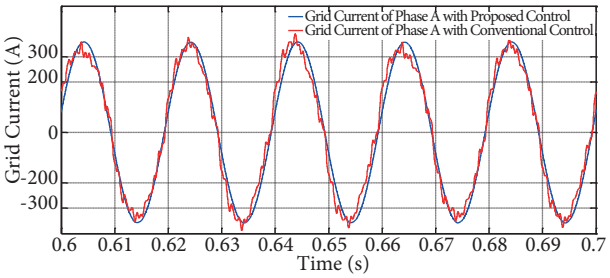

Figure 19. Waveform of Phase A grid current.

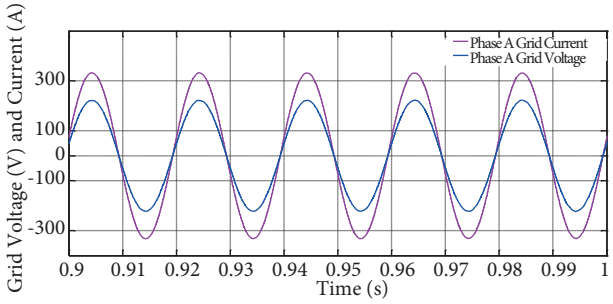

Figure 20. Waveform of Phase A grid current and voltage.

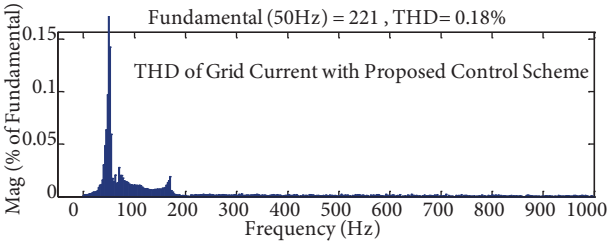

Figure 21. THD of grid current with proposed control scheme.

Phase A grid current is shown in Figure 19, where the waveforms clearly indicate that the proposed control scheme is able to effectively suppress the ripples while conventional control is not. However, Figure 20

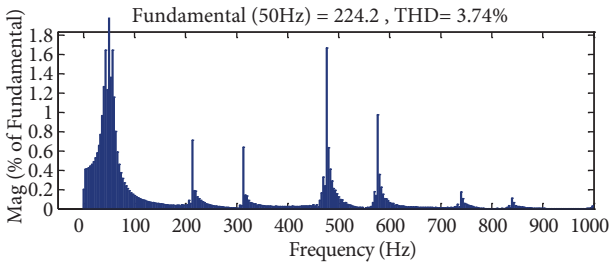

Figure 22. THD of grid current with conventional control scheme.

shows the effective control of reactive power to improve the power factor (P.F), where the P.F of the system at PCC is unity.

Figures 21 and 22 show the improved performance of the proposed control scheme as compared to the conventional control scheme in quantitative terms using total harmonic distortion (THD) of grid current as the performance parameter. THD in grid current with the proposed scheme is only 0.18%, whereas with the conventional scheme it is 3.71%. In both schemes, however, the THD is within limits as per IEEE standards, but the value of THD with the proposed control scheme is considerably reduced.

5. Conclusions

A novel control strategy has been proposed to improve power quality with the help of a SC. This paper has designed and analyzed the proposed control scheme to improve the dynamic response of a HES under weak grid conditions. Results of the HES have shown the improved and effective performance under transient as well as steady-state conditions in the weak grid environment. Comparative analysis of results with the conventional control scheme reveals that the transient and dynamic responses are improved considerably with the proposed scheme. Stability and robustness of the voltage as well as grid current controllers are improved under wide variations of grid inductance. Steady-state ripples in grid current are also damped out and hence waveform quality is improved. Besides the weak grid condition, the proposed control scheme has also improved the dynamic response under other operating conditions such as stiff grid, islanding, and overvoltage conditions. The proposed scheme may be extended further to improve the power quality under islanding microgrid environments in future work.

Nomenclature

U_{dc}	DC link voltage
C_{dc}	DC link capacitance
L_1, L_2	Filter inductance
C_f	Filter capacitance
U_{sabc}	Three-phase grid voltage
U_{gabc}	Three-phase voltage at PCC
R_g, L_g	Grid resistance and inductance
d_{sc}	Duty cycles of buck boost converter
i_{sc}, v_{sc}	SC current and voltage
i^*_{gd}, i^*_{gq}	Reference d- and q-axis grid current
i_{gd}, i_{gq}	d- and q-axis grid current
U_{gd}, U_{gq}	d- and q-axis grid voltage
U_{sd}, U_{sq}	d- and q-axis voltage at PCC
P_g	Power injected into the grid

P_{inv}	Input power of the inverter
i_{inv}	Inverter input current
i_{dc}	DC link capacitor current
U_d, U_q	d- and q-axis inverter output voltages
ω	Angular frequency
$\hat{i}_{gd}, \hat{i}_{gq}$	d- and q-axis ripple currents
U_d^*, U_q^*	d- and q-axis reference inverter voltages
f_s	Switching frequency
$\mathrm{G}_c(\mathrm{s})$	Gain of the outer current control loop
K_p	Gain of the inner current control loop
K_{pwm}	Gain of the inverter
$\mathrm{G}_v(\mathrm{s})$	Gain of PI voltage controller
$\mathrm{G}_{cl\_i}(\mathrm{s})$	Transfer function of the grid current closed loop control
$\mathrm{G}_{ol\_v}(\mathrm{s})$	Transfer function of the open loop voltage control
P.M., G.M.	Phase margin and gain margin
P_{comp}	Compensated power
i_{sc}^*	Reference SC current
$\mathrm{G}_{pi\_sc}(\mathrm{s})$	Gain of PI regulator of the SC control loop
$\mathrm{G}_{id\_sc}(\mathrm{s})$	Gain of bidirectional DC/DC buck-boost converter
$\mathrm{G}_{cl\_sc}(\mathrm{s})$	Closed loop transfer function of SC current control
$\mathrm{G}_{ol\_v}(\mathrm{s})$	Open loop transfer function of the proposed voltage control loop

References

[1] Sharma R, Sathans. Survey on hybrid (wind/solar) renewable energy system and associated control issues. In: Proceedings of the IEEE 6th India International Conference on Power Electronics; 8–10 December 2014; India. New York, NY, USA: IEEE. pp. 1-6.

[2] Nehrir H, Wang C, Strunz K, Aki H, Ramakumar R, Bing J, Miao Z, Salameh Z. A review of hybrid renewable/alternative energy systems for electric power generation: configurations, control, and applications. IEEE T Sustain Energy 2011; 2: 392-403.

[3] Han H, Hou X, Yang J, Wu J, Su M, Guerrero JM. Review of power sharing control strategies for islanding operation of AC microgrids. IEEE T Smart Grid 2016; 7: 200-215.

[4] Davari M, Mohamed YARI. Robust vector control of a very weak-grid-connected voltage-source converter considering the phase-locked loop dynamics. IEEE T Power Electr 2017; 32: 977-994.

[5] Pena-Alzola R, Liserre M, Blaabjerg F, Ordonez M, Yang YH. LCL-Filter design for robust active damping in grid-connected converters. IEEE T Ind Informa 2014; 10: 2192-2203.

[6] Tran TV, Chun TW, Lee HH, Kim HG, Nho EC. PLL-based seamless transfer control between grid-connected and islanding modes in grid-connected inverters. IEEE T Power Electr 2014; 29: 5218-5228.

[7] Xu JM, Xie SJ, Tang T. Improved control strategy with grid-voltage feedforward for LCL-filter-based inverter connected to weak grid. IET Power Electron 2014; 7: 2660-2671.

[8] Song Y, Nian H. Sinusoidal output current implementation of DFIG using repetitive control under a generalized harmonic power grid with frequency deviation. IEEE T Power Electr 2015; 30: 6751-6762.

[9] Zhang S, Jiang S, Lu X, Ge BM, Peng FZ. Resonance issues and damping techniques for grid-connected inverters with long transmission cable. IEEE T Power Electr 2014; 29: 110-120.

[10] Suul JA, D'Arco S, Rodríguez P, Molinas M. Impedance-compensated grid synchronisation for extending the stability range of weak grids with voltage source converters. IET Gener Transm Dis 2016; 10: 1315-1326.

[11] Chen X, Wang Y, Zhang Y, Chen J, Gong C. Impedance-phased dynamic control method for grid-connected inverters in a weak grid. IEEE T Power Electr 2017; 32: 274-283.

[12] Abusara M, Sharkh S, Zanchetta P. Adaptive repetitive control with feedforward scheme for grid-connected inverters. IET Power Electron 2015; 8: 1403-1410.

[13] Sun J. Small-signal methods for AC distributed power systems—A review. IEEE T Power Electr 2009; 24: 2545-2554.

[14] Egea-Alvarez A, Fekriasl S, Hassan F, Gomis-Bellmunt O. Advanced vector control for voltage source converters connected to weak grids. IEEE T Power Syst 2015; 30: 3072-3081.

[15] Huang Y, Yuan X, Hu J, Zhou P, Wang D. DC-bus voltage control stability affected by AC-bus voltage control in VSCs connected to weak AC grids. IEEE J Emerg Sel Top Power Electron 2016; 4: 445-458.

[16] Gee AM, Robinson FVP, Dunn RW. Analysis of battery lifetime extension in a small-scale wind-energy system using supercapacitors. IEEE T Energy Convers 2013; 28: 24-33.

[17] Reznik A, Simões GM, Al-Durra A, Muyeen SM. LCL filter design and performance analysis for grid-interconnected systems. IEEE Trans Ind Appl 2014; 50: 1225-1232.

[18] Xu J, Xie S, Tang T. Evaluations of current control in weak grid case for grid-connected LCL-filtered inverter. IET Power Electron 2013; 6: 227-234.

[19] Chen X, Wang Y, Zhang Y, Chen J, Gong C. Hybrid damping adaptive control scheme for grid-connected inverters in a weak grid. IET Power Electron 2016; 9: 2760-2768.

[20] Kollimalla SK, Mishra MK, Narasamma NL. Design and analysis of novel control strategy for battery and supercapacitor storage system. IEEE T Sustain Energy 2014; 5: 1137-1144.

[21] Chetrai S, Azli N, Ayob S, Mortezaei A. Design of a current mode PI controller for a single-phase PWM inverter. In: Proceedings of the IEEE Applied Power Electronics Colloquium; 18–19 April 2011; Johor Bahru, Malaysia. New York, NY, USA: IEEE. pp. 180-184.

[22] Jin Y, Xu J, Zhou G, Mi C. Small-signal modeling and analysis of improved digital peak current control of boost converter. In: Proceedings of the IEEE 6th International Power Electronics Motion Control Conference; 17–20 May 2009; China. New York, NY, USA: IEEE. pp. 326-330.